Pasanen, Toni; Vähänissi, Ville; Wolny, Franziska; Oehlke, Alexander; Wagner, Matthias; Juntunen, Mikko A.; Heikkinen, Ismo T. S.; Salmi, Emma; Sneck, Sami; Vahlman, Henri; Tolvanen, Antti; Hyvärinen, Jaakko; Savin, Hele

Industrial Applicability of Antireflection-Coating-Free Black Silicon on PERC Solar Cells and Modules

Published in:
Proceedings of the 35th European Photovoltaic Solar Energy Conference and Exhibition

DOI:
10.4229/35thEUPVSEC20182018-2AV.2.5

Published: 01/01/2018

Document Version
Publisher's PDF, also known as Version of record

Please cite the original version:
Pasanen, T., Vähänissi, V., Wolny, F., Oehlke, A., Wagner, M., Juntunen, M. A., Heikkinen, I. T. S., Salmi, E., Sneck, S., Vahlman, H., Tolvanen, A., Hyvärinen, J., & Savin, H. (2018). Industrial Applicability of Antireflection-Coating-Free Black Silicon on PERC Solar Cells and Modules. In *Proceedings of the 35th European Photovoltaic Solar Energy Conference and Exhibition* (pp. 552-556). EU PVSEC. https://doi.org/10.4229/35thEUPVSEC20182018-2AV.2.5

INDUSTRIAL APPLICABILITY OF ANTIREFLECTION-COATING-FREE BLACK SILICON ON PERC SOLAR CELLS AND MODULES

Toni P. Pasanen[1*], Ville Vähänissi[1], Franziska Wolny[2], Alexander Oehlke[2], Matthias Wagner[2], Mikko A. Juntunen[3], Ismo T. S. Heikkinen[1,4], Emma Salmi[4], Sami Sneck[4], Henri Vahlman[1,5], Antti Tolvanen[5], Jaakko Hyvärinen[5], and Hele Savin[1]

[1]Aalto University, Department of Electronics and Nanoengineering, Tietotie 3, 02150 Espoo, Finland
[2]SolarWorld Industries GmbH, Martin-Luther-King-Str. 24, 53175 Bonn, Germany
[3]Naps Solar Systems Inc., Ruosilankuja 4, 00390 Helsinki, Finland
[4]Beneq Oy, Olarinluoma 9, 02200 Espoo, Finland
[5]Endeas Oy, Ruukinkuja 1, 02330 Espoo, Finland

ABSTRACT: Black silicon (b-Si) is of particular interest within the photovoltaic community due to its ability to texture diamond wire-sawn multicrystalline silicon wafers. In this work, we apply a deep dry-etched black silicon nanotexture, which possesses less than 1 % solar-weighted reflectance with no antireflection coating (ARC), to industrial Passivated Emitter and Rear Cells (PERC). Additionally, the cells are processed further into small solar modules, which are characterized by their electrical and optical performance. The fragile nanostructures remain intact during industrial cell and module fabrication, maintaining the excellent optical properties until the final product. We show that b-Si modules with a typical cover glass retain their performance until incident angles larger than 60°, whereas the heavily increased reflectance of acidic-textured modules decreases their efficiency already after a 30° tilt. Furthermore, at an incidence angle of 70°, the efficiency of b-Si modules has reduced only 7 %, while that of the acidic-textured equivalents has decreased more than 25 %. Hence, the excellent optical properties of ARC-free b-Si are maintained also at module level. The results demonstrate that deep dry-etched b-Si nanostructures are fully applicable to current industrial PERC production facilities.
Keywords: black silicon, Passivated Emitter and Rear Cell, module, multicrystalline silicon, incidence angle

1 INTRODUCTION

Black silicon (b-Si) is currently highly topical for the PV industry due to its ability to eliminate reflective losses of diamond wire-sawn (DWS) multicrystalline silicon (mc-Si) wafers [1]. Indeed, the potential of b-Si as the next mainstream technology in the PV industry has been demonstrated as impressive b-Si cell results by several research groups [2-5]. A few b-Si fabrication methods, such as metal-assisted chemical etching (MACE) [6], have already demonstrated their industrial viability [7]. Although MACE clearly outperforms standard acidic texturing on DWS mc-Si wafers, the textured surfaces still typically require an antireflection coating (ARC) to decrease the surface reflectance to a sufficiently low level for high-efficiency solar cells [8, 9]. This is the case also with another promising b-Si fabrication method, atmospheric dry etching (ADE), where an excessively porous surface layer is removed after the ADE process by an additional polishing step [10], which changes surface morphology and increases reflectance.

The need for any ARC can be eliminated, and the optical properties improved further, by making b-Si nanostructures deeper, i.e., increasing their aspect ratio [11, 12]. Such surfaces can be fabricated e.g. via deep reactive ion etching (DRIE) [11], which is able to produce lattice defect-free deep b-Si nanostructures [13], eliminating the need for any post-etching polishing steps. In addition to increased performance, the application of deep b-Si would reduce cell manufacturing costs due to the exclusion of ARC deposition [14]. However, the larger height of b-Si increases the fragileness of the nanostructure, and only little effort has been made to study the applicability of deep dry-etched b-Si nanostructures to current industrial solar cell and module production lines. It remains ambiguous, whether the fragile nanostructure is damaged by wafer grippers or inline equipment, if screen-printing is applicable to deep b-Si, or how the b-Si affects the module encapsulation process. Moreover, the benefit from the excellent optical properties of deep b-Si may be partly diminished by ethylene vinyl acetate (EVA) and module cover glass [15].

In this contribution, we fabricate dry-etched b-Si Passivated Emitter and Rear Cells (PERC) at an industrial production line of SolarWorld Industries following the standard PERC process flow. The cells are processed further into small modules at the solar module factory of Naps Solar Estonia. The survival of b-Si is evaluated after various cell and module process steps, and the cells and modules are finally characterized by angle-dependent I-V measurements at the testing facility of Endeas.

2 EXPERIMENTAL METHODS

Industrial-sized (156 × 156 mm^2) mc-Si wafers were used as substrate material for the fabrication of b-Si PERC solar cells. The process flow followed the standard PERC process of SolarWorld Industries as applicable. First, a deep b-Si nanostructure (see inset in Fig. 1) was etched by DRIE on more than one hundred wafers using a process based on that reported in [11]. Due to clamping against the bottom electrode, approximately 5 mm from each wafer edge remained unetched. For reference purposes, some of the wafers were textured with the standard acidic texturing process in hydrofluoric-nitric acid (HF/HNO_3) solution [16].

Phosphorus emitter was formed by $POCl_3$ diffusion applying the same diffusion parameters for all wafers. After phosphosilicate glass (PSG) removal in HF, backside was passivated with a chemical-vapor-deposited (CVD) aluminum oxide/silicon nitride (AlO_x/SiN_x) stack. The acidic-textured cells were passivated with CVD SiN_x on the front according to the industry standard. Instead, the b-Si cells received an atomic-layer-deposited (ALD) AlO_x front surface passivation, since the conformality of CVD

layers is insufficient on deep b-Si [17]. Furthermore, AlO_x is the most widely studied ALD material [18] and has been demonstrated to passivate b-Si surfaces efficiently due to the high density of negative fixed charges and the high-quality interface with silicon [11, 13, 19]. The thin film conformality and the efficiency of surface passivation on deep dry-etched b-Si over the large 156 × 156 mm^2 wafer area was investigated by passivating a few non-diffused b-Si wafers with ALD AlO_x on both sides using the process reported in [20]. The lifetime samples were characterized by minority charge carrier lifetime using the microwave-detected photoconductance decay (μ-PCD) method. Finally, the cells were finished by an industry-standard screen-printing process of silver (Ag) metal contacts, which was followed by firing at 880 °C. Screen dimensions were adjusted to match with the b-Si area to have a uniform metal contact throughout the active cell area.

The prototype cell fabrication was kept as close to the industrial standard as possible at the industrial production line of SolarWorld Industries. However, b-Si was etched with a single-wafer equipment (Oxford Instruments Plasmalab System 100) at Aalto University, and AlO_x thin film for front surface passivation was deposited using a large-scale batch ALD tool (Beneq P400) at Beneq.

The efficiency of the finished cells was determined by current-voltage (I-V) measurements. The slightly smaller active area in the b-Si cells was taken into account in the data analysis. Additionally, the survival of the b-Si nanostructure was evaluated visually and by SEM after various process steps. Specifically, SEM characterization was focused on the evaluation of the metal-Si interface of screen-printed contacts. In addition, the optical properties of b-Si cells were examined by reflectance spectroscopy.

The cells, both b-Si and acidic-textured, were processed further into single-cell modules at the solar module factory of Naps Solar Estonia. All modules were fabricated using the same procedure. The untextured edges of the b-Si cells were removed by laser cutting prior to module encapsulation to have fully black solar modules. The acidic-textured cells were cut to equal size, which was approximately 146 × 146 mm^2. Electric contacts were established by regular tab wires, which were soldered manually to ensure better positioning of the wires on cut wafers. The encapsulation was performed simultaneously to both b-Si and acidic-textured modules using an industry-standard process. The modules had a standard PV glass, which was single-side textured and had no antireflection coating. Additionally, the strong cover glass was replaced in one module by a plastic cover, which is typically used in e.g. boat installations. This enabled the cutting of the module and cross-sectional inspection of the EVA – b-Si interface with SEM for the possibility of damaged nanostructure or air gaps inside the module. Finally, module efficiencies were measured as a function of incidence angle between 0° and 70°. The efficiency was calculated taking only the cell area into consideration to enable direct comparison between cell and module efficiencies. In addition, the effect of reducing solar irradiance with increasing incidence angle was cancelled out by calculations in the angle-dependent data.

3 RESULTS AND DISCUSSION

3.1 Optical and electrical properties of ARC-free b-Si

Figure 1 compares the measured reflectance spectra of ARC-free b-Si and standard acidic-textured cells with SiN_x ARC. While the reflectance of acidic-textured surfaces can be minimized efficiently at a certain wavelength with a proper ARC, deep dry-etched b-Si has negligible reflectance across the whole relevant solar spectrum range. This is contrary to the shallower "black silicon" surface textures currently utilized in the PV industry for DWS mc-Si, which still require separate polishing and ARC steps [8, 9]. The solar spectrum-weighted average reflectance of ARC-free b-Si cells is only 0.8 %, which is significantly lower than 8.3 % of AR-coated acidic-textured cells. Furthermore, the excellence of deep b-Si is even more emphasized in the ultraviolet range, where its reflectance is tens of percents lower than in standard cells (Fig. 1). Indeed, deep dry-etched b-Si studied here appears truly black to naked eye (Fig. 2a) due to the negligible reflectance, which eliminates the need for any ARC, and hence, reduces cell manufacturing costs [14].

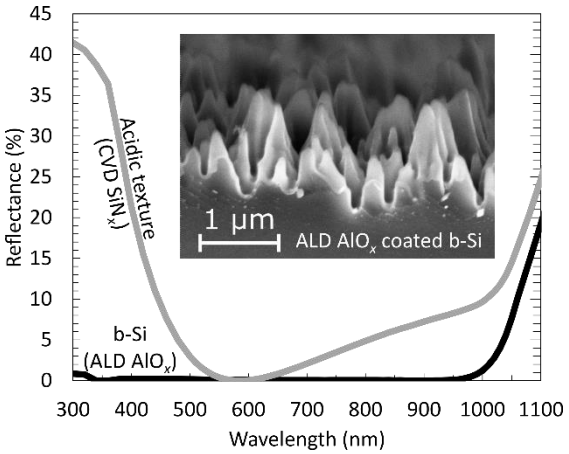

Figure 1: Surface reflectance of ARC-free b-Si solar cells with ALD AlO_x surface passivation and acidic-textured cells with standard SiN_x ARC. The solar spectrum-weighted average reflectance between 300 nm and 1000 nm of b-Si and acidic-textured cells is 0.8 % and 8.3 %, respectively. The inset presents a SEM image of the deep b-Si nanostructure coated conformally with ALD AlO_x.

Fortunately, the excellent optics do not have to come at the expense of electrical properties. Figure 2b shows a minority charge carrier lifetime map of a non-diffused b-Si wafer passivated with ALD AlO_x showing a high average lifetime of 250 μs. Separate grains are clearly visible in the map, indicating that the lifetime is limited by the bulk and the b-Si surface is efficiently passivated. Furthermore, the boundary of the b-Si area is not visible in the lifetime map, which further supports successful passivation throughout the 156 × 156 mm^2 area realized by a commercial batch ALD tool. The inset in Fig. 1 confirms that the deep b-Si nanostructures are indeed coated conformally with AlO_x, which is a prerequisite for efficient passivation. However, the efficiency of AlO_x surface passivation in the b-Si cells cannot directly be concluded from the lifetime results, since the cells have a phosphorus emitter at the front contrary to the lifetime samples, which will be discussed later in more detail.

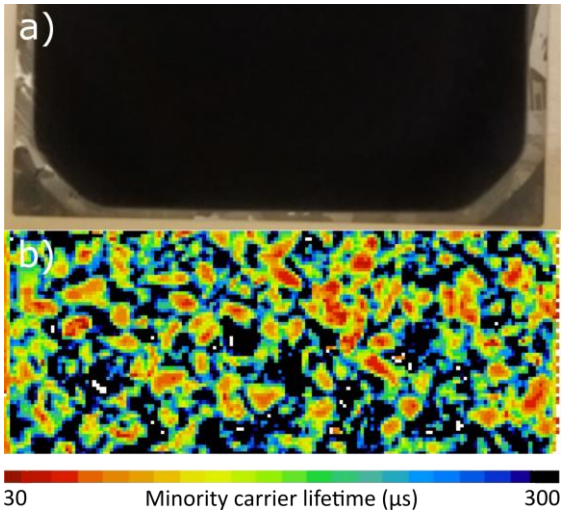

Figure 2: a) A photograph showing a half of a b-Si wafer with no ARC. Approximately 5 mm from each wafer edge remained unetched due to clamping against the bottom electrode during b-Si fabrication. b) Minority charge carrier lifetime map of the same b-Si wafer passivated with ALD AlO_x (average ~250 µs). Separate grains are clearly visible in the map, while the boundary of the b-Si area is invisible, indicating that the lifetime is limited by the bulk and b-Si surface is efficiently passivated.

3.2 Screen-printed contacts

Screen-printing is the current industry standard process for metal contact fabrication [1]. However, its applicability on deep b-Si is not obvious due to the high aspect ratio of the nanostructures. Nevertheless, earlier studies have promisingly reported that textured surfaces are in fact more compatible with contact formation by screen-printed Ag pastes than flat surfaces [21]. This is due to an increased available surface area for contacting and more optimal wetting of the dielectric, Si and Ag by the glass frit in the paste [21, 22]. The glass layer tends to concentrate in the valleys of the texture, enabling direct contact between the metal finger and Ag crystallites that form during the metallization process, which promotes low contact resistance [21, 22].

Figure 3a presents a SEM image of a screen-printed front contact finger of a b-Si cell fabricated in this work. Closer inspection reveals that the valleys between the nanostructures are indeed filled with the glass frit, whereas some b-Si tips are free of the thick insulating layer. This agrees with a previous study, which concluded that direct contacts between Si and Ag are the dominant current paths on b-Si surfaces [23]. Furthermore, the screen-printed metal finger and the Si – Ag interface on deep b-Si look rather similar to those on an acidic-textured surface (Fig. 3b), which suggests that the industrial metallization process is applicable also to b-Si. However, since screen-printing is performed through the front surface passivation film, the AlO_x layer needs to be thin enough (<10 nm) to avoid increased contact resistance [24]. Although the AlO_x film is too thin to be visible in the SEM image in Fig. 3a, it is expected that there is an insulating layer between Ag and Si, which increases contact resistance. Additionally, the performance of contacts is affected by the amount of inactive dopants and the depth of the highly-doped emitter region [23], which needs to be taken into consideration in the optimization of b-Si emitters [2, 12, 20].

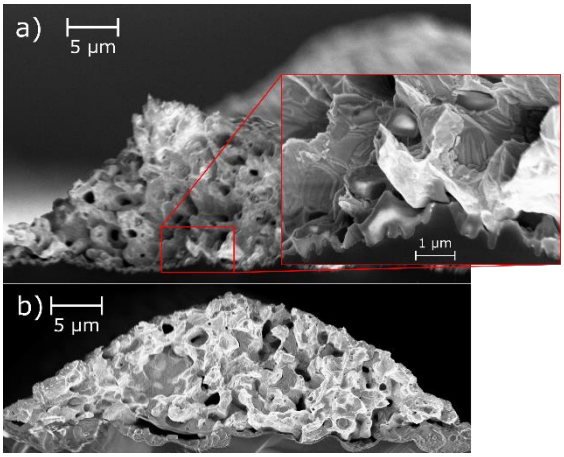

Figure 3: Screen-printed front contact finger on (a) b-Si coated with ALD AlO_x and (b) acidic-textured surface coated with SiN_x. The inset in figure (a) shows a zoomed view of the b-Si – metal interface.

3.3 Mechanical durability and module encapsulation

Visual and SEM inspection after various process steps reveals that the deep b-Si nanostructure remains intact during cell and module processing despite its fragile nature. No visible mechanical damage is produced to the b-Si by inline equipment or wafer grippers, which is an essential finding for the industrialization of the new technology.

Figure 4 presents a cross-sectional SEM image of an ARC-free b-Si module without cover glass. Mainly, no air gaps were observed at the EVA – b-Si interface, as preferred. However, a few micrometer-sized gaps were located, which allowed closer inspection of the nanostructures. The inset in Fig. 4 presents a SEM image taken from such gap, showing intact b-Si covered with EVA. Thus, the ARC-free nanostructure survives the encapsulation process, which is observed also as a deep black appearance of the finished modules (inset in Fig. 6).

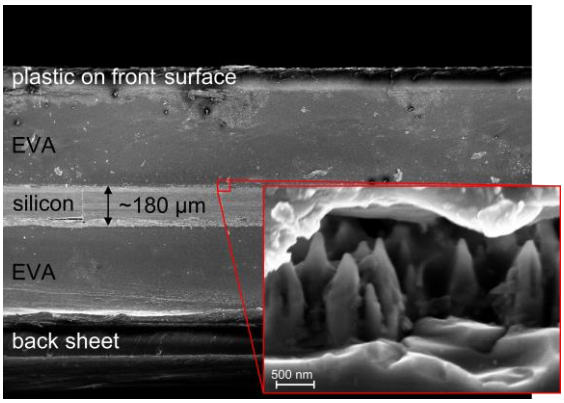

Figure 4: Cross-sectional structure of a b-Si solar module without glass. The inset presents a SEM image taken from a µm-scale gap at the ethylene vinyl acetate (EVA) – b-Si interface, which shows intact b-Si nanostructure covered with EVA.

3.4 Cell and module performance

The efficiencies of deep dry-etched b-Si and standard acidic-textured cells and modules are presented in Fig 5. The b-Si cells likely suffer from increased emitter losses due to an excessive amount of phosphorus in the heavily-doped layer [2, 12, 20]. This is a result of the application

of the standard emitter diffusion parameters to b-Si, which has significantly larger surface area. Moreover, the efficiency of the b-Si cells is partly limited due to the non-optimal charge polarity in ALD AlO_x for phosphorus emitter passivation [20, 25, 26]. Nevertheless, despite the above-mentioned hindrances, the excellent optics of deep b-Si raise the efficiency of the nanostructured cells to the same level with acidic-textured equivalents. Hence, higher efficiencies should be expected from deep b-Si cells after further optimization of emitter diffusion process for high aspect ratio nanostructures [2, 12, 20] and replacement of AlO_x e.g. with positively charged SiO_x/AlO_x stacks [20, 26, 27].

Although cell efficiencies heavily determine the module performance, the efficiency of modules is a more direct quantity for comparison between photovoltaic devices under real operating conditions. Figure 5 reveals that the efficiencies of both b-Si and acidic-textured devices are reduced by 2-3 $\%_{abs}$ at module level compared to the corresponding cell performance. This reduction can be mainly attributed to two factors. First, the modules have a single-side textured cover glass with no antireflection coating, which slightly increases the reflectance. Moreover, manual tab wire soldering caused additional losses in the metal contacts and the process generated cracks to both acidic-textured and b-Si cells. Consequently, the b-Si modules show slightly lower efficiency than the acidic-textured equivalents.

Nevertheless, efficiency measured immediately after fabrication may not directly reflect the device performance under real operating conditions. Indeed, a recent study showed that after prolonged usage, the b-Si cells should maintain their performance, whereas standard cells would likely suffer from Light- and Elevated Temperature-Induced Degradation [28]. Furthermore, the performance gain obtained by the application of b-Si could be emphasized when using dirtier substrate material, since b-Si getters detrimental impurities more effectively than flat surfaces [29]. Thirdly, the efficiency measured for perpendicular incident light neglects the ability of b-Si to absorb light that arrives at large incidence angles efficiently [4], which will be shown in the next section in more detail.

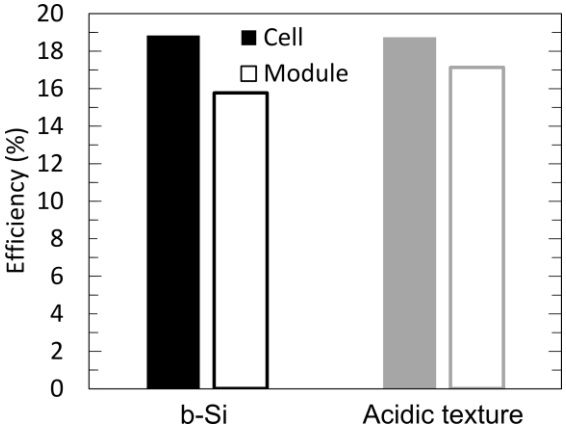

Figure 5: Power conversion efficiency of b-Si and acidic-textured PERC cells and modules. The efficiencies of b-Si cells are calculated considering only the active b-Si area.

3.5 Impact of incidence angle

Figure 6 presents the efficiency of b-Si and acidic-textured PERC modules as a function of light incident angle normalized to that of normal incidence. The reducing amount of solar irradiance arriving to the cell surface with increasing incidence angle (sketched in the inset) is cancelled out in the data by applying the equation presented in Fig. 6. The b-Si modules retain their performance until incident angles larger than 60°, whereas the efficiency of acidic-textured modules starts to decrease already after a 30° tilt due to heavily increased reflectance. This agrees well with earlier results reported at cell level [4]. Furthermore, at an incidence angle of 70°, the efficiency of b-Si modules has reduced only 7 %, while that of the acidic-textured equivalents has decreased more than 25 %. Hence, the results demonstrate that the excellent optical properties of deep ARC-free b-Si are maintained also at module level. This is an essential finding, since solar cells are always encapsulated, and hence, the cell level optics do not necessarily reflect the performance under real operating conditions.

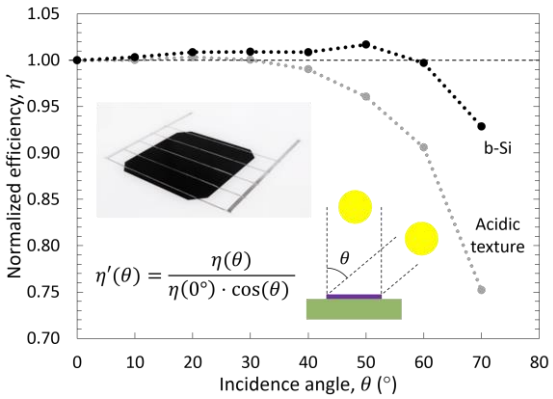

Figure 6: Incidence angle-dependent power conversion efficiency of b-Si and acidic-textured modules normalized to that of normal incidence. The effect of reducing solar irradiance with increasing incidence angle (sketched in the inset) is cancelled out in the data, as per the presented equation. The dotted lines act as a guide for eye. Values larger than unity can be accounted for measurement inaccuracy. The inset shows a photograph of a single-cell ARC-free b-Si solar panel.

4 CONCLUSIONS

This contribution demonstrated that deep dry-etched b-Si nanostructures, which possess less than 1 % solar-weighted reflectance with no ARC, survive well in industrial solar cell and module production, which has not been self-evident due to their fragile nature. Despite the lack of any polishing steps after b-Si etching, the nanostructure was efficiently passivated by a conformal ALD AlO_x thin film on the whole industrial-sized wafer area. Furthermore, the high aspect ratio of deep b-Si did not notably affect screen-printing. Instead, direct contact was formed between the emitter and silver finger on some b-Si tips, promoting good electrical contact. Finally, angle-dependent I-V measurements revealed that the b-Si modules retain their performance until an incidence angle of 60°, whereas the heavily increased reflectance of acidic-textured equivalents decreased their efficiency already after a 30° tilt. The results demonstrate that ARC-free b-Si is fully applicable to current PERC production facilities, and that the excellent deep b-Si optics are maintained also at module level. The main development area of the ARC-free b-Si technology is the upscaling of the dry etching

process to meet the demanding throughput requirement set by the PV industry.

ACKNOWLEDGEMENTS

The authors would like to thank Ander Pukk and Pavel Tšukrejev from Naps Solar Estonia for guidance in module assembly. The authors acknowledge the provision of facilities by Aalto University at OtaNano – Micronova Nanofabrication Centre. This work was funded by project "BLACK" (project No. 2956/31/2014), which was supported under the umbrella of SOLAR-ERA.NET by Business Finland (former Tekes – the Finnish Funding Agency for Innovation). T. P. Pasanen acknowledges the Aalto ELEC Doctoral School, Jenny and Antti Wihuri Foundation, and Walter Ahlström Foundation for the financial support.

REFERENCES

[1] International technology roadmap for photovoltaic: Results 2016. 8th Edition (2017).
[2] J. Oh, H.-C. Yuan, H. M. Branz, Nature Nanotechnology 7 (2012) 743.
[3] W.-C. Wang et al., Applied Materials & Interfaces 5 (2013) 9752.
[4] H. Savin et al., Nature Nanotechnology 10 (2015) 624.
[5] J. Benick et al., IEEE Journal of Photovoltaics 7 (2017) 1171.
[6] F. Toor et al., Nanoscale 8 (2016) 15448.
[7] B. Beetz, PV Magazine (2018) Available online: https://www.pv-magazine.com/2018/01/04/suntechs-black-silicon-solar-cells-enter-mass-production/ (accessed on May 30, 2018).
[8] Z. G. Huang et al., Solar Energy Materials & Solar Cells 143 (2015) 302.
[9] G. Su et al., Solar Energy 170 (2018) 95.
[10] P. Saint-Cast et al., Energy Procedia 124 (2017) 260.
[11] P. Repo et al., IEEE Journal of Photovoltaics 3 (2013) 90.
[12] B. Kafle et al., Solar Energy Materials & Solar Cells 152 (2016) 94.
[13] G. von Gastrow et al., Solar Energy Materials & Solar Cells 142 (2015) 29.
[14] C. Modanese, H. S. Laine, T. P. Pasanen, H. Savin, J. M. Pearce, Energies 11 (2018) 2337.
[15] J. Gjessing, E. S. Marstein, Energy Procedia 38 (2013) 348.
[16] A. Hauser, I. Melnyk, P. Fath, S. Narayanan, S. Roberts, T. M. Bruton, Proceedings of 3rd World Conference on Photovoltaic Energy Conversion, Osaka, Japan, 2 (2003) 1447.
[17] Y. Liu et al., Small 8 (2012) 1392.
[18] G. Dingemans, W. M. M. Kessels, Journal of Vacuum Science & Technology A 30 (2012) 040802.
[19] [Otto2012] M. Otto, M. Kroll, T. Käsebier, R. Salzer, A. Tünnermann, R. B. Wehrspohn, Applied Physics Letters 100 (2012) 191603.
[20] T. Pasanen, V. Vähänissi, N. Theut, H. Savin, Energy Procedia 124 (2017) 307.
[21] E. Cabrera et al,. Journal of Applied Physcis 110 (2011) 114511.
[22] E. Cabrera et al., IEEE Journal of Photovoltaics 3 (2013) 102.
[23] B. Kafle et al., IEEE Journal of Photovoltaics 7 (2017) 136.
[24] A. To, W. M. Li, X. Li, B. Hoex, Energy Procedia 124 (2017) 914.
[25] B. Hoex, J. J. H. Gielis, M. C. M. van de Sanden, W. M. M. Kessels, Journal of Applied Physics 104 (2008) 113703.
[26] B. W. H. van de Loo et al., Solar Energy Materials & Solar Cells 143 (2015) 450.
[27] B. W. H van de Loo, A. Ingenito, M. A. Verheijen, O. Isabella, M. Zeman, W. M. M. Kessels, Applied Physics Letters 110 (2017) 263106.
[28] T. P. Pasanen et al., Progress in Photovoltaics: Research and Applications, in peer review.
[29] T. P. Pasanen, H. S. Laine, V. Vähänissi, J. Schön, H. Savin, Scientific Reports 8 (2018) 1991.